

Review

The Evolution of Solid Oxide Fuel Cell Materials

Alexander Chroneos ^{1,2,*} , **Ioannis L. Goulatis** ¹, **Andrei Solovjov** ^{3,4} and **Ruslan V. Vovk** ⁴¹ Department of Electrical and Computer Engineering, University of Thessaly, 38333 Volos, Greece; yannislgoul@gmail.com² Department of Materials, Imperial College London, London SW7 2BP, UK³ B. I. Verkin Institute for Low Temperature Physics and Engineering of National Academy of Science of Ukraine, 47 Nauki Ave., 61103 Kharkiv, Ukraine; solovjov@ilt.kharkov.ua⁴ Department of Physics, V. N. Karazin Kharkiv National University, 4 Svobody Sq., 61077 Kharkiv, Ukraine; rvvovk2017@gmail.com

* Correspondence: alexander.chroneos@imperial.ac.uk; Tel.: +30-6978775320

Abstract: Solid oxide fuel cells (SOFCs) are a key component of the future energy landscape. Although there is considerable research on the physical properties and technology of classic oxide materials for electrode and electrolytes in SOFCs, the field is very active as new experimental and theoretical techniques are now available that can improve these systems. In the present review, we consider key systems such as perovskite-related materials, the impact of strain and interfaces and advanced concepts that can improve the properties of SOFC materials. In particular, we consider the oxygen diffusion properties of perovskite-related materials and focus on $\text{La}_2\text{NiO}_{4+\delta}$ and the double perovskites such as $\text{GdBaCo}_2\text{O}_{5.5}$. Then, we review the importance of interfaces and strain as a way to engineer defect processes. Finally, we consider advanced concepts to form designed structures that explore the effect of local high entropy on lattice stabilization.

Keywords: defect engineering; solid oxide fuel cells; atomistic simulation

Citation: Chroneos, A.; Goulatis, I.L.; Solovjov, A.; Vovk, R.V. The Evolution of Solid Oxide Fuel Cell Materials. *Appl. Sci.* **2024**, *14*, 69. <https://doi.org/10.3390/app14010069>

Academic Editors: Johannes Schwank and Aliaksandr Shaula

Received: 7 November 2023

Revised: 14 December 2023

Accepted: 18 December 2023

Published: 20 December 2023



Copyright: © 2023 by the authors. Licensee MDPI, Basel, Switzerland. This article is an open access article distributed under the terms and conditions of the Creative Commons Attribution (CC BY) license (<https://creativecommons.org/licenses/by/4.0/>).

1. Introduction

SOFCs have been considered for decades and have a vast number of applications including mobile (cars and buses) and industrial uses. In the past years, there has been a trend to introduce more efficient systems for energy conversion and storage and this includes SOFCs, batteries, supercapacitors, solar cells, etc. [1–25]. The main interest in SOFC technology is because of its very efficient energy conversion in conjunction with reduced emission of the so-called greenhouse gases as compared with the typical power generation routes [1,3]. Typically, SOFCs operate efficiently at high temperatures (up to 1000 °C), with hydrogen and fossil fuels converting chemical energy to electricity; however, they can also be used in combined heat and power applications [26,27]. A consequence of the high temperatures in which SOFCs operate is the high materials costs (materials issues include thermal cycling, chemical degradation, etc.) due to expensive interconnects and heat exchangers [28]. The impact of high temperature can be mitigated by lowering the operating temperatures to 500–700 °C (known as the intermediate temperature range). Nevertheless, SOFC thermal-activated processes (i.e., diffusion) are affected by the reduction in temperature, and this is particularly problematic for the cathode and electrolyte. This leads to the requirement of advanced materials with high rates of oxygen self-diffusion at these reduced temperatures. In particular, it is necessary to accelerate the oxygen diffusion in the cathode and electrolyte of the SOFC.

It should be stressed that the more conventional cathodes, for example, $\text{La}_{1-x}\text{Sr}_x\text{MnO}_{3-\delta}$, that are considered to be competent electronic conductors are not appropriate because of their low bulk ionic conductivity ([10] and references therein). This has led to the use of another group of materials called mixed ionic–electronic conductors (MIECs) as the oxygen reduction reaction (ORR) in MIEC electrodes is ruled by the oxygen surface exchange and

oxygen diffusion [10]. Similarly to cathodes, electrolytes for SOFCs also need to possess high ionic conductivity but with low electronic conductivity [10].

Oxygen diffusion is therefore fundamentally and technologically important for the cathode and electrolyte materials of SOFC [1–25]. Oxygen self-diffusion in these systems is a complicated phenomenon that is influenced by the composition, crystal structure, oxygen stoichiometry, doping and elastic strain ([10] and references therein). In that respect, predictive computational modelling can be used synergistically with experimental work to ensure an efficient design route for fast oxygen ion diffusion in SOFCs. Essentially, the complexities constitute the determination of the defect processes and the impact of various factors on these difficulties when using experiments and simulations at the atomic scale can offer detailed insights.

In this review, the focus is on the oxygen diffusion mechanisms of SOFC materials moving from more common materials (perovskite-related materials) to novel concepts, considering the latter emphasis is given on recent theoretical (refer to Section 2.2) and associated experimental results highlighting the importance of strain, interfaces and architectures on the enhancement of the diffusion properties of oxide materials for SOFC applications.

2. Methodology

2.1. Recent Developments

In the past decades there has been more intensive use of experimental and theoretical techniques. In particular, the advancement of secondary ion mass spectrometry (SIMS) (and variants such as time-of-flight (ToF) SIMS) has led to the very precise determination of self- and dopant diffusion in energy and electronic materials [29,30]. From a theoretical viewpoint, the development of molecular dynamics (MD) and density functional theory (DFT) in conjunction with ever-increasing computational resources is a powerful and complementary tool [31–34]. It is a complementary tool given that atomistic simulations can more efficiently quantify migration energy barriers and point defect processes at different planes and directions [35–39]. If these techniques are combined with advanced techniques such as cluster expansion and special quasirandom structures (SQS), structurally and compositionally complicated systems can be considered [40–55]. Finally, thermodynamic techniques including the $cB\Omega$ model by Varotsos and Alexopoulos can benefit from the understanding of the point defect chemistry and provide predictions for a vast range of temperatures and pressures [56–62].

2.2. Atomistic Simulation

The most common ways to investigate the defect processes on SOFC materials at the atomistic level is via classical MD and DFT, as has been shown in previous theoretical studies [63–70]. Classical MD has been a popular way to investigate the atomic scale properties of inorganic materials for over 40 years. The present computational resources allow the MD simulations of many millions of atoms and therefore research can include extended defects such as grain boundaries. This is important as polycrystalline material processes can be dominated or severely impacted at the extended defects. Classical MD is a fairly simple method where the state of the system is predicted by considering the positions and the momenta of the particles using Newton's equations of motion, which are solved iteratively in order to calculate the evolution of the system. Interparticle interactions are described using the potential energy function. For SOFC, the ionic systems are modelled within the classical Born-like description [71,72]. Typically, the ionic interactions can be modelled by a Coulombic term (long-range) and by a short-range parameterized pair potential [73,74]. Although MD calculations in ionic systems can work very well and can be a useful tool when considering dynamical properties such as diffusion, they cannot calculate the electronic structure of the system.

When considering electronic properties, DFT calculations are advantageous over MD. It is acknowledged that the quantum mechanical description is the most complete depiction of nature. What is also acknowledged is that the analytic solution of the Schrödinger

equation for practical systems (i.e., a substantial number of electrons and nuclei) is intractable due to the complexity of many-electron interactions [75–77]. The DFT method was discovered to address these issues via the description of the exchange-correlation energy of electrons through approximations (typically the local density approximation (LDA), the generalized gradient approximation (GGA) or with hybrid functionals) [75,76]. A key aspect of DFT is to use a plane-wave basis set with the pseudopotential method, where the core electrons can be modelled by effective potentials and the valence electrons can evolve explicitly [75–77]. Although DFT is at zero kelvin and diffusion typically occurs at high temperatures, there are ways to gain information for the energetics of diffusion using this approach. For example, formation energies (the energy to form a point defect) of ionic systems can be easily modelled, whereas for the activation energy of migration (i.e., the energy barrier that the ion has to overcome to move from one minimum energy site to the next), methods such as the nudged elastic band method can be employed. An issue with the DFT study of ionic materials is the supercell size, as it needs to be extended enough so that periodic images have little effect upon the calculated energies. This is particularly important for extended and charged defects. Finally, it should be considered that the ab initio MD can overcome many of the problems of classical MD (for example, the inability to calculate electronic properties) and DFT (i.e., it is dynamic and can model high temperatures); however, it is a technique that is very computationally intensive, so it is typically limited to small number of atoms.

3. Materials Systems

3.1. Perovskite-Related Materials

Perovskite and perovskite-related materials are particularly important for a range of applications from SOFC to high-temperature superconductivity [78–87]. For example, the community has investigated the $\text{ReBa}_2\text{Cu}_3\text{O}_{7-\delta}$ (where Re = rare earth element or Y) system following the discovery of high-temperature superconductivity [78]. Through doping and external conditions, these systems showed improvements in the critical temperature of superconductivity (T_c) [80,81]. In fact, these systems are still also being investigated for fusion applications [85–87]. Regarding materials for SOFC lanthanum nickelate ($\text{La}_2\text{NiO}_{4+\delta}$), gadolinium barium cobaltate ($\text{GdBaCo}_2\text{O}_{5+\delta}$) and other perovskite-related systems have been considered in the past two decades [29,35,88–100].

Considering first oxygen self-diffusion in $\text{La}_2\text{NiO}_{4+\delta}$, it should be considered that the experimental determination of its energetics and mechanism is difficult due to its crystal structure and oxygen hypo- or hyperstoichiometry. For example, it was difficult to determine the energetics and mechanism of oxygen self-diffusion in $\text{La}_2\text{NiO}_{4+\delta}$ [10,29]. Experimental time-of-flight secondary ion mass spectrometry investigations on $\text{La}_2\text{NiO}_{4+\delta}$ by Sayers et al. [29] determined an activation energy of oxygen migration of 0.54–0.56 eV in excellent agreement with the classical MD work (0.51 eV [89]). MD also revealed that the dominant oxygen self-diffusion mechanism in $\text{La}_2\text{NiO}_{4+\delta}$ is the interstitialcy mechanism (in the a–b plane) in which oxygen interstitials displace apical oxygens from the NiO_6 octahedron, which are thereafter promoted to adjacent oxygen interstitial sites [89].

Although praseodymium (Pr) has a very negative effect in perovskite-related high- T_c superconductivity, Pr-based perovskite materials such as $\text{PrBaCo}_2\text{O}_{5+\delta}$ or $\text{Pr}_2\text{NiO}_{4+\delta}$ were considered by the SOFC community due to their high oxygen self-diffusion [90,93]. In the intermediate temperature range, $\text{Pr}_2\text{NiO}_{4+\delta}$, similarly to the isostructural $\text{La}_2\text{NiO}_{4+\delta}$, has a tetragonal crystal structure (I4/mmm space group, refer to Figure 1a). This structure can be described as perovskite layers (PrNiO_3) intergrown with rock salt layers (PrO) [90]. There is a mismatch between the layers which leads to the introduction of oxygen interstitials in the Pr_2O_2 bilayers [90]. This, in turn, leads to the local distortion of the NiO_6 octahedra (refer to Figure 1a) due to the Coulombic repulsion between the oxygen interstitial and the apical ions in the NiO_6 octahedra [89]. This effect is key if the aim is to understand the mechanism of oxygen self-diffusion of $\text{Pr}_2\text{NiO}_{4+\delta}$ at the atomic level. The interstitialcy oxygen self-diffusion mechanism in the a–b plane in $\text{Pr}_2\text{NiO}_{4+\delta}$ is common with related

systems such as $\text{La}_2\text{NiO}_{4+\delta}$, as mentioned above, and $\text{La}_2\text{CoO}_{4+\delta}$ [92]. Figure 1a is based on classical MD calculations and shows the isosurface connecting the oxygen diffusion sites in the a–b plane [90]. This isosurface is in agreement with the maximum entropy method results reported in a related system (Figure 1b, reference [90] and references therein).

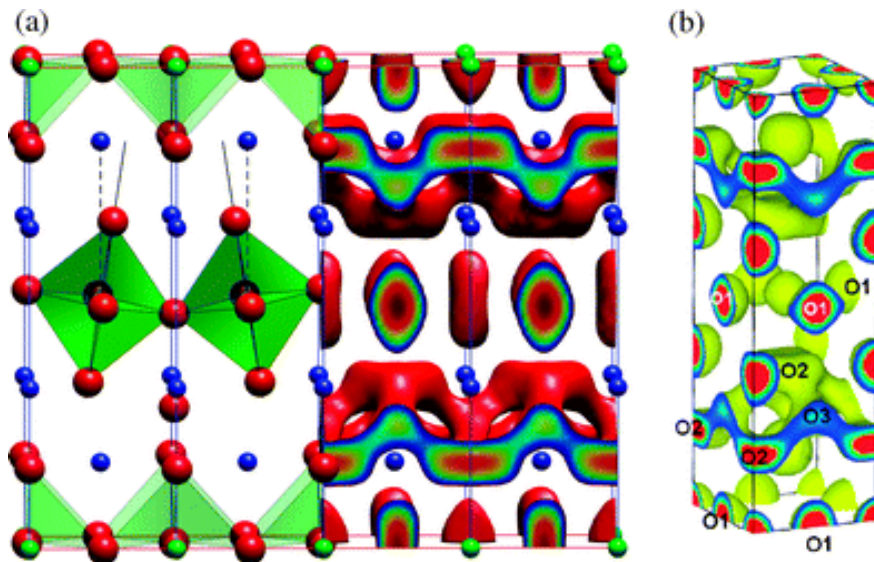


Figure 1. The structure and oxygen self-diffusion in $\text{Pr}_2\text{NiO}_{4+\delta}$. (a) The crystal structure, where NiO_6 octahedra are green, Ni ions are blue and O ions are red (c -axis is the vertical axis); MD calculations at 1100 K and $\delta = 0.09875$ predicting the isosurface of the O diffusion sites (in the a – b plane) and (b) maximum entropy method results [90].

The community has also investigated the impact of intrinsic point defects such as antisites on the diffusion properties in perovskite materials for SOFCs. An interesting example is $\text{GdBaCo}_2\text{O}_{5+\delta}$ (double perovskite structure), which has high oxygen diffusivity with an activation energy of 0.5 eV [91]. In ordered $\text{GdBaCo}_2\text{O}_{5+\delta}$, oxygen self-diffusion is highly anisotropic and takes place primarily in the Gd–O and adjacent Co–O layers [91]. This is shown using MD results in Figure 2a [91]. What the MD results by Parfitt et al. [91] showed is that cation disorder in the Gd–Ba sublattice will result in a decrease in the oxygen diffusivity with the diffusion becoming more isotropic (there is now significant diffusion in the c -axis). Figure 2c quantifies the differences in the oxygen self-diffusion in the c -axis and the a – b plane with respect to the level of cation disorder [91]. In the left y -axis of this figure is the ratio of the diffusivity in the c -axis over the diffusivity in the a – b plane, whereas the right y -axis represents the total diffusivity [91]. The x -axis corresponds to the antisite disorder, i.e., the ratio of Gd atoms occupying a Ba site over the Gd atoms occupying a Ba or Gd lattice site. Considering the zero of the x -axis, that is when there is no antisite disorder, there is in essence no diffusivity in the c -axis (anisotropic diffusion) [91], whereas the total diffusivity (predominantly in the a – b plane) is maximum [91]. At the other extreme (i.e., for the x -axis value of 0.5) where there is maximum antisite disorder, the total diffusivity is minimized, whereas the left y -axis is nearly 1 (i.e., diffusion becomes isotropic) [91]. What can be deduced is that cation disorder in the double perovskites will minimize oxygen self-diffusion [91]. Therefore, for SOFCs, these systems should be ordered and oriented in a way that they benefit from the maximum oxygen diffusion in the a – b plane. In essence, cation antisite disorder is a design parameter that can be used to tune the energetics of diffusion and direct the diffusion mechanism. The key findings and activation energies for the perovskite-related materials considered here are summarized in Table 1.

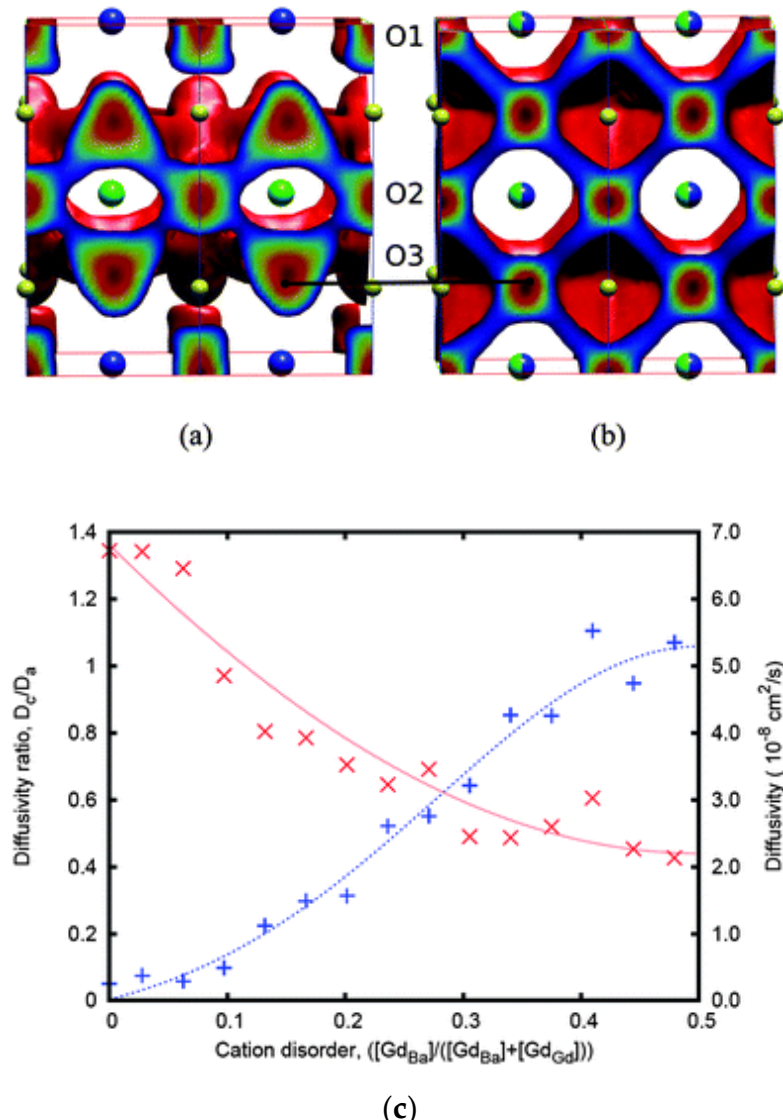


Figure 2. (a) Classical MD results of the oxygen diffusion pathways in (a) ordered and (b) disordered GdBaCo₂O_{5.5} for $\delta = 0.5$ at $T = 900$ K. (c) The ratio of diffusivities in the a- and c-axis (D_c/D_a represented by + and the blue line) with respect to the cation disorder for $\delta = 0.5$ at $T = 1200$ K. The second y-axis represents the diffusivity values (×, red line) with respect to the cation disorder [91].

Table 1. The activation energies of oxygen diffusion and comments on the mechanism of oxygen diffusion in representative oxides.

Material	Activation Energy/eV	Comments
La ₂ NiO _{4+δ}	0.51	[29], Classical MD, anisotropic mechanism along the a–b plane, interstitialcy mechanism
La ₂ NiO _{4+δ}	0.54–0.56	[29], Experiment
GdBaCo ₂ O _{5+δ}	0.50	[91] Classical MD, anisotropic mechanism along the a–b plane. Cation antisite disorder retards diffusion, makes it more isotropic
Sr _{0.75} Y _{0.25} CoO _{2.625}	1.56	[8], Classical MD, isotropic mechanism, vacancy mechanism

3.2. Interfaces and Strain

Understanding the impact of strain and interfaces is key for the development of more efficient and sustainable materials for SOFC applications [101–110]. The intriguing study of Garcia-Barriocanal et al. [4] determined that in nanostructured $\text{SrTiO}_3/\text{YSZ}/\text{SrTiO}_3$ heterostructures, there is colossal conductivity. In particular, in this heterostructure, yttria stabilized zirconia (ZrO_2 with 8 mol% Y_2O_3) layers under 7% tensile strain have conductivities eight orders of magnitude higher than bulk YSZ [4]. This extreme enhancement in ionic conductivity was treated with skepticism from the community but it nevertheless led to numerous studies in $\text{SrTiO}_3/\text{YSZ}/\text{SrTiO}_3$ and related heterostructures [5,9,103,104]. Cavallaro et al. [103] determined that in the $\text{SrTiO}_3/\text{YSZ}/\text{SrTiO}_3$ heterostructure, the total conductivity dependence is inconsistent with ionic diffusion in YSZ, whereas the DFT work by Kushima and Yildiz [9] in biaxially strained bulk YSZ predicted ionic enhancement by up to four orders of magnitude. Notably, in that study, the migration energy barriers were calculated using the nudged elastic band (NEB) method in relatively small supercells [9]. What is profound in the studies following the work by Garcia-Barriocanal et al. [4] is that tensile strain does significantly increase ionic conductivity but this does not translate to an eight-order of magnitude increase in ionic diffusion. Nevertheless, there is increased interest in the oxygen diffusion properties at oxide interfaces [105–109]. Lee et al. [24] employed ionic interfaces to produce a nonstoichiometric oxygen vacancy concentration. This in turn is very important as oxygen vacancy concentrations at equilibrium are limited, and, therefore, there is a requirement to increase their content as oxygen vacancies are the vehicles of oxygen diffusion in these systems. Lee et al. [24] used the oxide nanobrush architecture to form a substantial nonequilibrium oxygen vacancy concentration at the interface between CeO_2 and Y_2O_3 . This is an important example of how the material architecture (here, the designed interfacial oxide) can be used to increase the formation and tune the diffusion properties of defects. With a similar objective but with a more fundamentally scientific viewpoint, the investigation by Chiabrera et al. [22] showed that the modification of nonstoichiometry in grain boundaries can be employed to tune the diffusion properties. Chiabrera et al. [22] effectively determined that point defects induced by strain in the grain boundaries of $\text{La}_{1-x}\text{Sr}_x\text{MnO}_{3\pm\delta}$ increase the oxygen diffusivity and diminish the electronic and magnetic order.

Kuganathan et al. [109] employed static atomistic simulations to examine the minimum energy oxygen diffusion pathways and activation migration energies at the STO–LCO interface (refer to Figure 3). It was predicted by these calculations that curved pathways have lower migration energies [109]. Kuganathan et al. [109] showed that at the Sr–Cr–La interface layer, the fastest oxygen transport occurs along the a-axis (i.e., in the Cr layer) with an activation energy of migration of 0.36 eV. This migration energy is significantly smaller than the 0.53 eV calculated for oxygen diffusion in bulk LCO using the same methodology [109]. Considering the c-axis of the Cr layer, the activation energy of migration for oxygen is 0.48 eV, i.e., lower by only 0.05 eV as compared to the activation energy of migration in LCO bulk [109]. Therefore, oxygen will preferentially diffuse along the a-axis in the interface layer. In the La–Cr–Sr layer, the b-axis oxygen activation energy of migration is 0.60 eV, which is not significantly lower than the activation energy of migration (0.64 eV) calculated in bulk STO [109]. Finally, at the Sr–Ti–La interface layer, the activation energies of migration predicted along the a-axis and the c-axis in the Ti layer are lower by about 0.10 eV as compared to bulk STO [99]. At the b-axis of the Sr–Ti–La layer, there is a considerable increase in the activation energy of migration in comparison to bulk STO (by 0.04 eV) or bulk LCO (by 0.15 eV) [109].

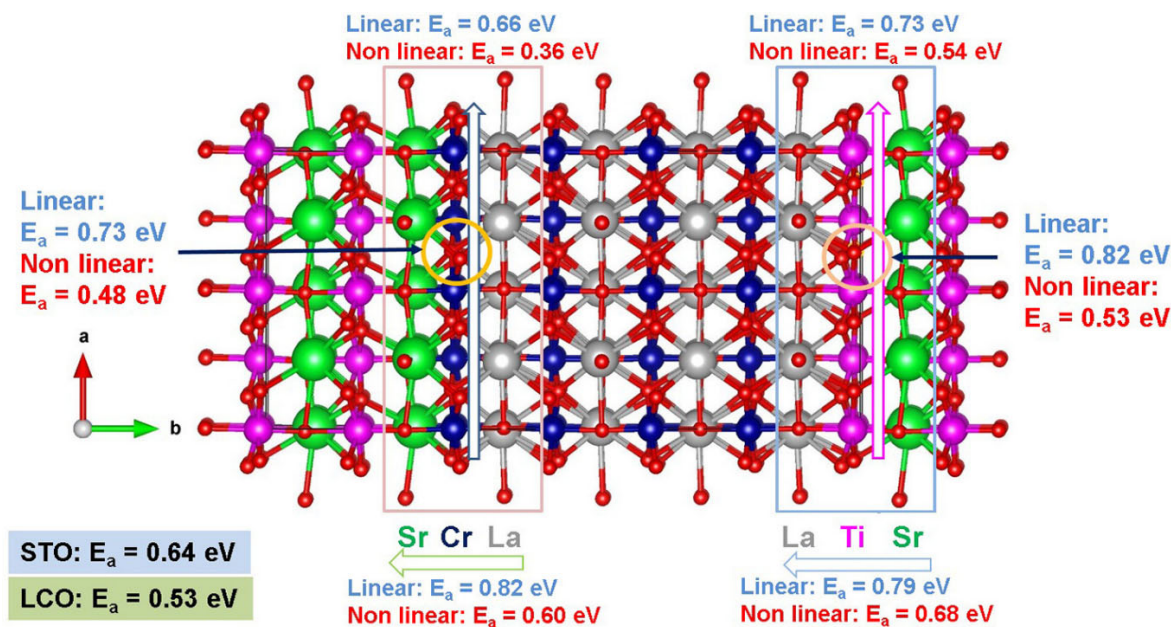


Figure 3. Static atomistic simulation results of the activation energies of migration calculated in the STO–LCO interface [109].

3.3. Advanced Concepts

In order to attain improved performance and downscaling so as to be compatible with the design specifications that will be required, solid oxide cells (SOC) need to benefit from beyond-state-of-the-art concepts for nanoengineering materials [111]. In essence, practical applications will need to approach the scaling rate of Moore’s Law as it has been observed in microelectronics for many decades. In reality, this is hindered by the poor thermochemical stability, limited electrode catalytic activity and the difficulties in the efficient introduction of nanoscale materials, all of which undermine the use of SOCs as a portable energy source. The improvement of the SOC air electrode can be achieved using scarce materials or by the introduction of advanced ceramic nanostructures formed using mixed ionic–electronic conducting oxides (MIECs) such as doped cobaltites, ferrites and manganites [112]. It is critical in MIEC materials to balance the free energy of the oxygen redox cycle and the enthalpy of oxide reduction as this will ensure significant electrocatalytic activity over the free surface combined with enhanced oxygen diffusion [113]. In thin-film MIECs, the dense microstructure leads to significant in-plane percolation, and the potential of nanostructuring through cutting-edge thin-film techniques is a way to unravel nanoscale effects (i.e., fast oxygen reduction kinetics diffusion) [23]. MIEC thin films are beneficial for SOC functional layers as they do not have areas with high oxygen chemical potential gradients or high electronic current density that are deleterious for device performance; however, there are still issues that need to be considered such as dopant segregation toward the surface that can lead to limited thermal stability [114]. Controlling and limiting cation self-diffusion is important to limit the formation of insulating secondary phases and also to retain surface activity in the long term [115,116]. The community has addressed the improvement of MIEC thin films’ performance through chemical doping, inclusion of interfaces, surface decoration and strain engineering [117–121]. The difficulty that emerges is to mitigate cation segregation and to improve the oxygen reduction reaction (ORR) kinetics [122].

To improve the oxygen diffusion at intermediate temperatures, MIEC can be paired with oxygen conductors to form nanocomposites, with applications as SOC electrodes and dual-phase membranes for oxygen separation. Nanocomposites are structurally stable and have the benefit of ionic and electronic species transport [123,124]. Vertically aligned nanostructures (VANs) are considered as an alternative to the nanocomposite electrode functional

layers [125]. VANs have been studied for nearly a decade and, in particular, nanocolumn in matrix mesostructures exhibited important functionalities such as controlled resistive switching, enhanced ionic diffusion and photocatalytic properties [126–129]. The interplay of interfacial effects (elastic strain ionic and electronic redistribution) inspired the investigation of self-assembled MIEC–fluorite thin-film vertical nanocomposites for applications in SOFCs [37,130,131]. The benefit of these studies is the realization of the VAN approach; however, their inclusion of inert model substrates and unrealistic electrolyte layers leads to incoherent interfaces with low interface density, and these in turn restrain the potential of VANs and inhibit their use in realistic electrochemical devices. The recent study by Baiutti et al. [25] described the construction of a self-assembled thin-film VAN nanocomposite using an electronic conductor ($\text{La}_{0.8}\text{Sr}_{0.2}\text{MnO}_3$ (LSM)) and an ionic conductor ($\text{Ce}_{0.8}\text{Sm}_{0.2}\text{O}_2$ (SDC)). Importantly, VAN has long-range order and phase alternation with nanosized column width ($\approx 10\text{ nm}$) [25]. Using a yttria-stabilized zirconia (YSZ) electrolyte as support, this nanostructure is compatible as a functional oxide nanomaterial for high-temperature electrochemical devices (i.e., as a SOC functional electrode layer given the high stability against cation migration and accelerated ORR kinetics) [132]. Importantly, the introduction of nano-engineered composite oxides can lead to further ways for the development of new functional materials with improved electrochemical properties [25].

Interestingly, the Baiutti et al. study [25] employed DFT calculations to study the effects of local high entropy on lattice stabilization. In particular, they used spin-polarized DFT on a confined cubic perovskite supercell (refer to Figure 4), aiming to gain insights into the thermal stability of the LSM-SDC VAN. This is not trivial; however, the study focused on the high degree of cation (Sm and Ce) intermixing. The ability of DFT to decouple between the different contributions and to quantify energy and strain differences is valuable to gain insights that are not feasible via experiment. The study by Baiutti et al. [25] showed that the determined isotropic compressive strain of LSM in the VAN structure is due to the introduction of Sm from the SDC layers. Importantly, spontaneous cation interdiffusion leads to Sr segregation suppression, whereas LSM can be considered a six-element high-entropy oxide [25]. This is also consistent with the results by Yang et al. [133], who have determined entropy-induced stabilization for bulk LSM. Figure 4 illustrates the DFT-derived results, showing the lattice strain due to doping, the mean and distribution of site volumes around the La and Sr sites and the bond valence mismatch of the ionic positions for the different cation dopants [25]. In $\text{La}_{0.875}\text{Sr}_{0.125}\text{MnO}_3$, it is predicted that the Sr ion is significantly overbonded (i.e., the surrounding oxygen ions are closer), whereas La ions are slightly underbonded [25]. This valence mismatch in conjunction with electrostatic effects can be key for the exchange of overbonded Sr ions with underbonded La ions on the surface [25]. This incoherency is balanced by cationic intermixing (refer to Figure 4c,d) [25]. The incorporation of Ce will effectively increase the Sr–O site volume and reduce the Sr–O overbonding compared to the La–O polyhedral [25]. This will result in a decrease in the elastic driving force for Sr surface segregation. That is, the configurational entropy increase leads to more stable LSM via local lattice distortion, consistent with theoretical studies [25,134]. VAN structures are (a) self-assembled and therefore their composition and interfaces at a growth temperature are thermodynamically stable, and (b) they can accommodate Ce contents beyond the solubility limit [25,135].

In essence, the whole approach is based on using VANs for the combination of the very good oxygen exchange properties of LSM and the fast oxygen diffusion of SDC to form an advanced designed electrode functional layer for SOCs. The heavily codoped manganite phase in the VAN is a high-entropy oxide which is stable and obstructs Sr segregation from the surface. The consequence is very long-term durability. The study by Baiutti et al. [25] determined (via isotopic exchange depth profiling based on APT) that there is a fast oxygen diffusion pathway along the SDC phase. This is a paradigm of the use of VAN nanocomposites as a tool to fix current kinetic limitations of existing electrodes. The VAN architecture is relatively easy to form and leads to prolonged thermal stability and fast oxygen reduction kinetics [25,136–138].

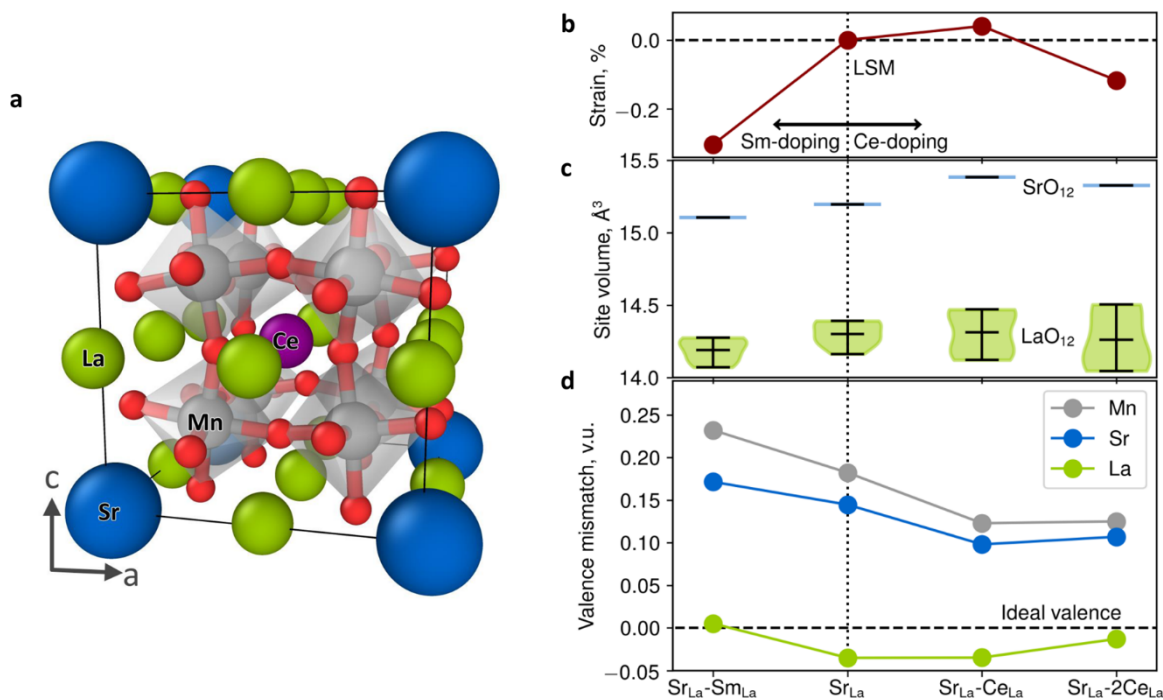


Figure 4. DFT-derived results illustrating (a) the relaxed positions of the Mn (gray), Sr (blue), La (green), O (red) and Ce (purple) ion in the 40-atom periodic supercell $\text{La}_{0.75}\text{Sr}_{0.125}\text{Sm}_{0.125}\text{MnO}_3$. (b) The predicted lattice strain due to doping, (c) the mean and distribution of site volumes around the La (green) and Sr (blue) sites and (d) bond valence mismatch of the ionic positions for the different cation dopants [25].

3.4. Perspectives

It should be stressed that this review is not exhaustive but rather aimed at highlighting some key SOFC materials, properties and theoretical ways to predict them. The research community is very active on these systems, as can be seen through the very high publication rate (refer for example to [99,100,139–152] and references therein).

4. Summary and Future Outlook

In the present energy landscape, there is increased need for efficient energy conversion combined with reduced emissions, and this is where SOFC technology thrives. Although typical material systems for these technologies have been investigated for decades, there has been renewed interest in the past few years as SOFCs can play a more mainstream role, and there is the desire to move to intermediate temperatures and hence more advanced materials that can operate efficiently at these lower temperatures. The investigations in the past 20 years have benefited from the advanced computational techniques (and substantial computational power) and the advances in experimental techniques (for example, ToF-SIMS). Presently, experiment and theory are synergistically employed, as they can provide complementary information that can accelerate progress and guide the community to more fruitful systems. The computational techniques allow the prediction of the point defect processes, early recognition of defect engineering strategies, the diffusion mechanisms and energetics. Commonly, the quest for more efficient SOFC research is focused on compositionally and structurally complicated materials.

The community is working towards a path for the development of next-generation functional oxides for SOFC and electrochemical applications. Vertically aligned nanostructures can be used to form electrode functional layers for SOFCs, taking advantage of the excellent oxygen exchange properties of LSM in conjunction with the good diffusivity of SDC. With the spontaneous formation of a high entropy oxide in the VAN, a stable compound is formed, which limits cation segregation to the surface, increasing

the long-term durability of solid oxide electrochemical cells. It is determined that VAN nanocomposites can solve kinetic limitations of electrodes and, in general, can be an efficient strategy for oxide electrochemistry (combining fast oxygen reduction kinetics with long-term thermal stability).

What is also important is to avoid expensive, unsustainable and scarce materials, which can be a bottleneck for the use of the technology. It is common in research to use rare earths and other expensive materials; however, the limitations in the production and their availability require a reduction in the dependence on these materials. In this respect, the use of more efficient architectures such as VAN to improve properties is very positive. Whatever the technological solutions, the future development of energy conversion, storage and production systems will require the understanding and optimization of all intermediate steps from cradle to grave.

Author Contributions: The manuscript was written and edited by all authors. All authors have read and agreed to the published version of the manuscript.

Funding: The research leading to these results has received funding from the European Union's H2020 Programme under Grant Agreement no. 824072—HARVESTORE.

Institutional Review Board Statement: Not applicable.

Informed Consent Statement: Not applicable.

Data Availability Statement: Not applicable.

Conflicts of Interest: The authors declare no conflict of interest.

References

1. Singhal, S.C. Advances in solid oxide fuel cell technology. *Solid State Ion.* **2000**, *135*, 305–313. [[CrossRef](#)]
2. Sata, N.; Eberman, K.; Eberl, K.; Maier, J. Mesoscopic fast ion conduction in nanometre scale planar heterostructures. *Nature* **2000**, *408*, 946–949. [[CrossRef](#)]
3. Steele, B.C.H.; Heinzel, A. Materials for fuel-cell technologies. *Nature* **2001**, *414*, 345–352. [[CrossRef](#)] [[PubMed](#)]
4. Garcia-Barriocanal, J.; Rivera-Calzada, A.; Varela, M.; Sefrioui, Z.; Iborra, E.; Leon, C.; Pennycook, S.J.; Santamaría, J. Colossal ionic conductivity at interfaces of epitaxial $ZrO_2:Y_2O_3/SrTiO_3$ heterostructures. *Science* **2008**, *321*, 676–680. [[CrossRef](#)] [[PubMed](#)]
5. Kilner, J.A. Ionic conductors: Feel the strain. *Nat. Mater.* **2008**, *7*, 838. [[CrossRef](#)] [[PubMed](#)]
6. Guo, X. Comment on “Colossal ionic conductivity at interfaces of epitaxial $ZrO_2:Y_2O_3/SrTiO_3$ heterostructures”. *Science* **2009**, *324*, 5926. [[CrossRef](#)]
7. Schichtel, N.; Korte, C.; Hesse, D.; Janek, J. Elastic strain at interfaces and its influence on ionic conductivity in nanoscaled solid electrolyte thin films- theoretical considerations and experimental studies. *Phys. Chem. Chem. Phys.* **2009**, *11*, 3043–3048. [[CrossRef](#)]
8. Rupasov, D.; Chroneos, A.; Parfitt, D.; Kilner, J.A.; Grimes, R.W.; Istomin, S.Y.; Antipov, E.V. Oxygen diffusion in $Sr_{0.75}Y_{0.25}CoO_{2.625}$: A molecular dynamics study. *Phys. Rev. B Condens. Matter* **2009**, *79*, 172102. [[CrossRef](#)]
9. Kushima, A.; Yildiz, B. Oxygen ion diffusivity in strained yttria stabilized zirconia: Where is the fastest strain? *J. Mater. Chem.* **2010**, *20*, 4809–4819. [[CrossRef](#)]
10. Chroneos, A.; Yildiz, B.; Tarancón, A.; Parfitt, D.; Kilner, J.A. Oxygen diffusion in solid oxide fuel cell cathode and electrolyte materials: Mechanistic insights from atomistic simulations. *Energy Environ. Sci.* **2011**, *4*, 2774–2789. [[CrossRef](#)]
11. Yang, Y.; Fei, H.; Ruan, G.; Xiang, C.; Tour, J.M. Edge-oriented MoS_2 nanoporous films as flexible electrodes for hydrogen evolution reactions and supercapacitor devices. *Adv. Mater.* **2014**, *23*, 8163–8168. [[CrossRef](#)] [[PubMed](#)]
12. Chesnaud, A.; Braida, M.D.; Estrade, S.; Peiro, F.; Tarancón, A.; Morata, A.; Dezanneau, G. High-temperature anion and proton conduction in RE_3NbO_7 ($RE = La, Gd, Y, Yb, Lu$) compounds. *J. Eur. Ceram. Soc.* **2015**, *35*, 3051–3061. [[CrossRef](#)]
13. Tarancón, A.; Morata, A. New insights into the origin of the oxide ionic diffusion change in strained lattices of yttria stabilized zirconia. *Comput. Mater. Sci.* **2015**, *103*, 206–215. [[CrossRef](#)]
14. Yun, S.; Zhou, X.; Even, J.; Hagfeldt, A. Theoretical treatment of $CH_3NH_3PbI_3$ perovskite solar cells. *Angew. Chem.* **2017**, *56*, 15806–15817. [[CrossRef](#)] [[PubMed](#)]
15. Lambert, D.S.; Murphy, S.T.; Lennon, A.; Burr, P.A. Formation of intrinsic and silicon defects in MoO_3 under varied oxygen partial pressure and temperature conditions: An ab initio DFT investigation. *RSC Adv.* **2017**, *7*, 53810–53821. [[CrossRef](#)]
16. Dahlqvist, M.; Petruhins, A.; Lu, J.; Hultman, L.; Rosen, J. Origin of chemically ordered atomic laminates (i-MAX): Expanding the elemental space by a theoretical/experimental approach. *ACS Nano* **2018**, *12*, 7761–7770. [[CrossRef](#)]
17. Kuganathan, N.; Iyngaran, P.; Vovk, R.; Chroneos, A. Defects, dopants and Mg diffusion in $MgTiO_3$. *Sci. Rep.* **2019**, *9*, 4394. [[CrossRef](#)]

18. Ning, D.; Baki, A.; Scherb, T.; Song, J.; Fantin, A.; Liu, X.Z.; Schumacher, G.; Banhart, J.; Bouwmeester, H.J.M. Influence of A-site deficiency on structural evolution of $\text{Pr}_{2-x}\text{NiO}_{4+\delta}$ with temperature. *Solid State Ion.* **2019**, *342*, 115056. [[CrossRef](#)]
19. Shi, J.; Han, C.; Niu, H.; Zhu, Y.; Yun, S. Theoretical investigation of proton diffusion in Dion-Jacobson layered perovskite $\text{RbBiNb}_2\text{O}_7$. *Nanomaterials* **2021**, *11*, 1953. [[CrossRef](#)]
20. Griesammer, S.; Belova, I.V.; Murch, G.E. Thermodiffusion and ion transport in doped ceria by molecular dynamics simulations. *Acta Mater.* **2021**, *210*, 116802. [[CrossRef](#)]
21. Wang, F.; Xing, Y.; Hu, E.; Wang, J.; Shi, J.; Yun, S.; Zhu, B. PN heterostructure interface-facilitated proton conduction in 3C-SiC/ $\text{Na}_{0.6}\text{CoO}_2$ electrolyte for fuel cell application. *ACS Appl. Energy Mater.* **2021**, *4*, 7519–7525. [[CrossRef](#)]
22. Chiabrera, F.; Garbayo, I.; Lopez-Conesa, L.; Martin, G.; Ruiz-Caridad, A.; Walls, M.; Ruiz-Gonzalez, L.; Kordatos, A.; Nunez, M.; Morata, A.; et al. Engineering transport in manganites by tuning local nonstoichiometry in grain boundaries. *Adv. Mater.* **2019**, *31*, 1805360. [[CrossRef](#)] [[PubMed](#)]
23. Acosta, M.; Baiutti, F.; Tarancón, A.; MacManus-Driscoll, J.L. Nanostructured materials and interfaces for advanced ionic electronic conducting oxides. *Adv. Mater. Interfaces* **2019**, *6*, 1900462. [[CrossRef](#)]
24. Lee, D.; Gao, X.; Sun, L.; Jee, Y.; Poplawsky, J.; Farmer, T.O.; Fan, L.; Guo, E.-J.; Lu, Q.; Heller, W.T.; et al. Colossal oxygen vacancy formation at a fluorite-bixbyite interface. *Nat. Commun.* **2021**, *11*, 1371. [[CrossRef](#)] [[PubMed](#)]
25. Baiutti, F.; Chiabrera, F.; Acosta, M.; Diercks, D.; Parfitt, D.; Santiso, J.; Wang, X.; Cavallaro, A.; Morata, A.; Wang, H.; et al. A high-entropy manganite in an ordered nanocomposite for long-term application in solid oxide cells. *Nat. Commun.* **2021**, *12*, 2660. [[CrossRef](#)]
26. Minh, N.Q.; Takahashi, T. *Science and Technology of Ceramic Fuel Cells*; Elsevier: Amsterdam, The Netherlands, 1995.
27. Fleig, J. Solid oxide fuel cell cathodes: Polarization mechanisms and modeling of the electrochemical performance. *Annu. Rev. Mater. Res.* **2003**, *33*, 361–382. [[CrossRef](#)]
28. Jacobson, A.J. Materials for solid oxide fuel cells. *Chem. Mater.* **2010**, *22*, 660–674. [[CrossRef](#)]
29. Sayers, R.; De Souza, R.A.; Kilner, J.A.; Skinner, S.J. Low temperature diffusion and oxygen stoichiometry in lanthanum nickelate. *Solid State Ion.* **2010**, *181*, 386–391. [[CrossRef](#)]
30. Kube, R.; Bracht, H.; Hansen, J.L.; Larsen, A.N.; Haller, E.E.; Paul, S.; Lerch, W. Composition dependence of Si and Ge diffusion in relaxed $\text{Si}_{1-x}\text{Ge}_x$ alloys. *J. Appl. Phys.* **2010**, *107*, 073520. [[CrossRef](#)]
31. Smith, W.; Forester, T.R. DL_POLY_2.0: A general-purpose parallel molecular dynamics simulation package. *J. Mol. Graph.* **1996**, *14*, 136. [[CrossRef](#)]
32. Gale, J.D. GULP: A computer program for the symmetry-adapted simulation of solids. *J. Chem. Soc. Faraday Trans.* **1997**, *93*, 629. [[CrossRef](#)]
33. *Computer Modelling in Inorganic Crystallography*; Catlow, C.R.A. (Ed.) Academic Press: San Diego, CA, USA, 1997.
34. Segall, M.D.; Lindan, P.J.D.; Probert, M.J.; Pickard, C.J.; Hasnip, P.J.; Clark, S.J.; Payne, M.C. First-principles simulation: Ideas, illustrations and the CASTEP code. *J. Phys. Condens. Matter* **2002**, *14*, 2717. [[CrossRef](#)]
35. Seymour, I.D.; Chroneos, A.; Kilner, J.A.; Grimes, R.W. Defect processes in orthorhombic $\text{LnBaCo}_2\text{O}_{5.5}$ double perovskites. *Phys. Chem. Chem. Phys.* **2011**, *13*, 15305–15310. [[CrossRef](#)] [[PubMed](#)]
36. Yildiz, B. “Stretching” the energy landscape of oxides- Effects on eletrocatalysis and diffusion. *MRS Bull.* **2014**, *39*, 147–156. [[CrossRef](#)]
37. Ma, W.; Kim, J.J.; Tsvetkov, N.; Daio, T.; Kuru, Y.; Cai, Z.; Chen, Y.; Sasaki, K.; Tuller, H.L.; Yildiz, B. Vertically aligned nanocomposite $\text{La}_{0.8}\text{Sr}_{0.2}\text{CoO}_3$ / $(\text{La}_{0.5}\text{Sr}_{0.5})_2\text{CoO}_4$ cathodes—Electronic structure, surface chemistry and oxygen reduction kinetics. *J. Mater. Chem. A* **2015**, *3*, 207–219. [[CrossRef](#)]
38. King, D.M.; Middleburgh, S.C.; Edwards, L.; Lumkin, G.R.; Cortie, M. Predicting the crystal structure and phase transitions in high-entropy alloys. *JOM* **2015**, *67*, 2375–2380. [[CrossRef](#)]
39. Kuganathan, N.; Rushton, M.J.D.; Grimes, R.W.; Kilner, J.A.; Gkanas, E.I.; Chroneos, A. Self-diffusion in garnet-type $\text{Li}_7\text{La}_3\text{Zr}_2\text{O}_{12}$ solid electrolytes. *Sci. Rep.* **2021**, *11*, 451. [[CrossRef](#)]
40. Sanchez, J.M.; Ducastelle, F.; Gratias, D. Generalized cluster description of multicomponent systems. *Phys. A Stat. Mech. Its Appl.* **1984**, *128*, 334–350. [[CrossRef](#)]
41. Zunger, A.; Wei, S.H.; Ferreira, L.G.; Bernard, J.E. Special quasirandom structures. *Phys. Rev. Lett.* **1990**, *65*, 353–356. [[CrossRef](#)]
42. Wei, S.H.; Ferreira, L.G.; Bernard, J.E.; Zunger, A. Electronic properties of random alloys: Special quasirandom structures. *Phys. Rev. B Condens. Matter* **1990**, *42*, 9622–9649. [[CrossRef](#)]
43. Laks, D.B.; Ferreira, L.G.; Froyen, S.; Zunger, A. Efficient cluster expansion for substitutional systems. *Phys. Rev. B Cover. Condens. Matter Mater. Phys.* **1992**, *46*, 12587–12605. [[CrossRef](#)] [[PubMed](#)]
44. Wolverton, C.; Zunger, A. Ising-like description of structurally released ordered and disordered alloys. *Phys. Rev. Lett.* **1995**, *75*, 3162–3165. [[CrossRef](#)] [[PubMed](#)]
45. Zunger, A.; Wang, L.G.; Hart, G.L.W.; Sanati, M. Obtaining Ising-like expansions for binary alloys from first principles. *Model. Simul. Mater. Sci. Eng.* **2002**, *10*, 685–706. [[CrossRef](#)]
46. Jiang, C.; Sordelet, D.J.; Gleeson, B. First-principles study of phase stability in pseudobinary $(\text{Ni}_{1-x}\text{Pt}_x)_3\text{Al}$ alloys. *Phys. Rev. B Cover. Condens. Matter Mater. Phys.* **2005**, *72*, 184203. [[CrossRef](#)]
47. Chroneos, A.; Jiang, C.; Grimes, R.W.; Schwingenschlögl, U.; Bracht, H. Defect interactions in $\text{Sn}_{1-x}\text{Ge}_x$ alloys. *Appl. Phys. Lett.* **2009**, *94*, 252104. [[CrossRef](#)]

48. Chroneos, A.; Jiang, C.; Grimes, R.W.; Schwingenschlögl, U.; Bracht, H. E centers in $\text{Si}_{1-x-y}\text{Ge}_x\text{Sn}_y$ alloys. *Appl. Phys. Lett.* **2009**, *95*, 112101. [[CrossRef](#)]
49. Chroneos, A.; Bracht, H.; Jiang, C.; Überuaga, B.P.; Grimes, R.W. Nonlinear stability of E centers in $\text{Si}_{1-x}\text{Ge}_x$: Electronic structure calculations. *Phys. Rev. B* **2008**, *78*, 195201. [[CrossRef](#)]
50. Christopoulos, S.R.G.; Kuganathan, N.; Chroneos, A. Electronegativity and doping $\text{Si}_{1-x}\text{Ge}_x$ alloys. *Sci. Rep.* **2020**, *10*, 7459. [[CrossRef](#)]
51. Jiang, C.; Wolverton, C.; Sofo, J.; Chen, L.Q.; Liu, Z.K. First-principles study of binary bcc alloys using special quasirandom structures. *Phys. Rev. B* **2004**, *69*, 214202. [[CrossRef](#)]
52. Dahlqvist, M.; Rosen, J. The rise of MAX phase alloys—Large-scale theoretical screening for the prediction of chemical order and disorder. *Nanoscale* **2022**, *14*, 10958–10971. [[CrossRef](#)]
53. Murphy, S.T.; Chroneos, A.; Grimes, R.W.; Jiang, C.; Schwingenschlögl, U. Phase stability and the arsenic vacancy defect in $\text{In}_x\text{Ga}_{1-x}\text{As}$. *Phys. Rev. B* **2011**, *84*, 184108. [[CrossRef](#)]
54. Jiang, C. First-principles study of ternary bcc alloys using special quasi-random structures. *Acta Mater.* **2009**, *57*, 4716–4726. [[CrossRef](#)]
55. Lumley, S.C.; Grimes, R.W.; Murphy, S.T.; Burr, P.A.; Chroneos, A.; Chard-Tuckey, P.R.; Wenman, M.R. The thermodynamics of hydride precipitation: The importance of entropy, enthalpy and disorder. *Acta Mater.* **2014**, *79*, 351–362. [[CrossRef](#)]
56. Varotsos, P. Calculation of the migration volume of vacancies in ionic solids from macroscopic parameters. *Phys. Status Solidi* **1978**, *47*, K133–K136. [[CrossRef](#)]
57. Varotsos, P.; Alexopoulos, K. *Thermodynamics of Point Defects and Their Relation with the Bulk Properties*; North-Holland: Amsterdam, The Netherlands, 1986.
58. Varotsos, P. Comparison of models that interconnect point defect parameters in solids with bulk properties. *J. Appl. Phys.* **2007**, *101*, 123503. [[CrossRef](#)]
59. Zhang, B.; Wu, X.; Xu, J.; Zhou, R. Application of the cBΩ model for the calculation of oxygen self-diffusion coefficients in minerals. *J. Appl. Phys.* **2010**, *108*, 053505. [[CrossRef](#)]
60. Cooper, M.W.D.; Grimes, R.W.; Fitzpatrick, M.E.; Chroneos, A. Modeling oxygen self-diffusion in UO_2 under pressure. *Solid State Ion.* **2015**, *282*, 26–30. [[CrossRef](#)]
61. Chroneos, A.; Vovk, R.V. Modeling self-diffusion in UO_2 and ThO_2 by connecting point defect parameters with bulk properties. *Solid State Ion.* **2015**, *274*, 1–3. [[CrossRef](#)]
62. Skordas, E.S.; Sarlis, N.V.; Varotsos, P.A. Applying the cBΩ thermodynamical model to LiF using its equation of state obtained from high pressure diamond anvil cell measurements. *Solid State Ion.* **2020**, *354*, 115404. [[CrossRef](#)]
63. Sickafus, K.E.; Minervini, L.; Grimes, R.W.; Valdez, J.A.; Ishimaru, M.; Li, F.; McClellan, K.J.; Hartmann, T. Radiation tolerance of complex oxides. *Science* **2000**, *289*, 748–751. [[CrossRef](#)]
64. Stanek, C.R.; Grimes, R.W.; Rushton, M.J.D.; McClellan, K.J.; Rawlings, R.D. Surface dependent segregation of Y_2O_3 in t-ZrO₂. *Phil. Mag. Lett.* **2005**, *85*, 445–453. [[CrossRef](#)]
65. De Souza, R.A.; Ramadan, A.; Hörner, S. Modifying the barriers for oxygen-vacancy migration in fluorite-structured CeO₂ electrolytes through strain; A computer simulation study. *Energy Environ. Sci.* **2012**, *5*, 5445–5453. [[CrossRef](#)]
66. Jay, E.E.; Rushton, M.J.D.; Grimes, R.W. Migration of fluorine in fluorapatite—A concerted mechanism. *J. Mater. Chem.* **2012**, *22*, 6097–6103. [[CrossRef](#)]
67. Rushton, M.J.D.; Chroneos, A.; Skinner, S.J.; Kilner, J.A.; Grimes, R.W. Effect of strain on the oxygen diffusion in yttria and gadolinia co-doped ceria. *Solid State Ion.* **2013**, *230*, 37–42. [[CrossRef](#)]
68. Rushton, M.J.D.; Chroneos, A. Impact of uniaxial strain and doping on oxygen diffusion in CeO₂. *Sci. Rep.* **2014**, *4*, 6068. [[CrossRef](#)] [[PubMed](#)]
69. Marrocchelli, D.; Sun, L.; Yildiz, B. Dislocation in SrTiO₃: Easy to reduce but not so fast for oxygen transport. *J. Am. Chem. Soc.* **2015**, *137*, 4735–4748. [[CrossRef](#)] [[PubMed](#)]
70. Kuganathan, N.; Chroneos, A. Defects, diffusion, dopants and encapsulation of Na in $\text{NaZr}_2(\text{PO}_4)_3$. *Materialia* **2021**, *16*, 101039. [[CrossRef](#)]
71. Born, M.; Mayer, J.E. Zur Gittertheorie der Ionenkristalle. *Z. Phys.* **1932**, *75*, 1–18. [[CrossRef](#)]
72. Buckingham, R.A. The classical equation of state of gaseous helium, neon and argon. *Proc. R. Soc. Lond. Ser. A* **1938**, *168*, 264.
73. Busker, G.; Grimes, R.W.; Bradford, M.R. The diffusion of iodine and caesium in the $\text{UO}_{2\pm x}$ lattice. *J. Nucl. Mater.* **2000**, *279*, 46–50. [[CrossRef](#)]
74. Busker, G.; Grimes, R.W.; Bradford, M.R. The solution and diffusion of ruthenium in $\text{UO}_{2\pm x}$. *J. Nucl. Mater.* **2003**, *312*, 156–162. [[CrossRef](#)]
75. Hohenberg, P.; Kohn, W. Inhomogeneous electron gas. *Phys. Rev.* **1964**, *136*, B864. [[CrossRef](#)]
76. Kohn, W. Nobel Lecture: Electronic structure of matter—Wave functions and density functionals. *Rev. Mod. Phys.* **1998**, *71*, 1253. [[CrossRef](#)]
77. Koch, W.; Holthausen, M.C. *A Chemist's Guide to Density Functional Theory*; Wiley-VCH: Weinheim, Germany, 2001.
78. Bednorz, J.G.; Mueller, K.A. Possible high T_c superconductivity in the Ba-La-Cu-O system. *Z. Phys. B Condens. Matter* **1988**, *64*, 189–193. [[CrossRef](#)]

79. Vovk, R.V.; Obolenskii, M.A.; Zavgorodniy, A.A.; Bondarenko, A.V.; Goulati, I.L.; Samoilov, A.V.; Chroneos, A. Effect of high pressure on the fluctuation conductivity and the charge transfer of $\text{YBa}_2\text{Cu}_3\text{O}_{7-\delta}$ single crystals. *J. Alloys Compd.* **2008**, *453*, 69–74. [[CrossRef](#)]
80. Vovk, R.V.; Obolenskii, M.A.; Bondarenko, A.V.; Goulati, I.L.; Samoilov, A.V.; Chroneos, A.; Simoes, V.M.P. Transport anisotropy and pseudo-gap state in oxygen deficient $\text{ReBa}_2\text{Cu}_3\text{O}_{7-\delta}$ ($\text{Re} = \text{Y}, \text{Ho}$) single crystals. *J. Alloys Compd.* **2008**, *464*, 58–66. [[CrossRef](#)]
81. Vovk, R.V.; Obolenskii, M.A.; Zavgorodniy, A.A.; Goulati, I.L.; Beletskii, V.I.; Chroneos, A. Structural relaxation, metal-to-insulator transition and pseudo-gap in oxygen deficient $\text{HoBa}_2\text{Cu}_3\text{O}_{7-\delta}$ single crystals. *Phys. C Supercond.* **2009**, *469*, 203–206. [[CrossRef](#)]
82. Vovk, R.V.; Nazyrov, Z.F.; Obolenskii, M.A.; Goulati, I.L.; Chroneos, A.; Simoes, V.M.P. Phase separation in oxygen deficient $\text{HoBa}_2\text{Cu}_3\text{O}_{7-\delta}$ single crystals: Effect of pressure and twin boundaries. *Phil. Mag.* **2011**, *91*, 2291–2302. [[CrossRef](#)]
83. Vovk, R.V.; Obolenskii, M.A.; Nazyrov, Z.F.; Goulati, I.L.; Chroneos, A.; Simoes, V.M.P. Electro-transport and structure of 1-2-3 HTSC single crystals with different plane defect topologies. *J. Mater. Sci. Mater. Electron.* **2012**, *23*, 1255–1259. [[CrossRef](#)]
84. Solov'ev, A.L.; Tkachenko, M.A.; Vovk, R.V.; Chroneos, A. Fluctuation conductivity and pseudogap in $\text{HoBa}_2\text{Cu}_3\text{O}_{7-\delta}$ single crystals under pressure with transport current flowing under an angle 45° to the twin boundaries. *Phys. C Supercond.* **2014**, *501*, 24–31. [[CrossRef](#)]
85. Murphy, S.T. A point defect model for $\text{YBa}_2\text{Cu}_3\text{O}_7$ from density functional theory. *J. Phys. Commun.* **2020**, *4*, 115003. [[CrossRef](#)]
86. Gray, R.L.; Rushton, M.J.D.; Murphy, S.T. Molecular dynamics simulations of radiation damage in $\text{YBa}_2\text{Cu}_3\text{O}_7$. *Supercond. Sci. Technol.* **2022**, *35*, 035010. [[CrossRef](#)]
87. Torsello, D.; Gambino, D.; Gozzelino, L.; Trotta, A.; Laviano, F. Expected radiation environment and damage for YBCO tapes in compact fusion reactors. *Supercond. Sci. Technol.* **2023**, *36*, 014003. [[CrossRef](#)]
88. Tarancón, A.; Skinner, S.J.; Chater, R.J.; Hernandez-Ramirez, F.; Kilner, J.A. Layered perovskites as promising cathodes for intermediate temperature solid oxide fuel cells. *J. Mater. Chem.* **2007**, *17*, 3175. [[CrossRef](#)]
89. Chroneos, A.; Parfitt, D.; Kilner, J.A.; Grimes, R.W. Anisotropic oxygen diffusion in tetragonal $\text{La}_2\text{NiO}_{4+\delta}$: Molecular dynamics calculations. *J. Mater. Chem.* **2010**, *20*, 266–270. [[CrossRef](#)]
90. Parfitt, D.; Chroneos, A.; Kilner, J.A.; Grimes, R.W. Molecular dynamics study of oxygen diffusion in $\text{Pr}_2\text{NiO}_{4+\delta}$. *Phys. Chem. Chem. Phys.* **2010**, *12*, 6834–6836. [[CrossRef](#)] [[PubMed](#)]
91. Parfitt, D.; Chroneos, A.; Tarancón, A.; Kilner, J.A. Oxygen ion diffusion in cation ordered/disordered $\text{GdBaCo}_2\text{O}_{5+\delta}$. *J. Mater. Chem.* **2011**, *21*, 2183–2186. [[CrossRef](#)]
92. Kushima, A.; Parfitt, D.; Chroneos, A.; Yildiz, B.; Kilner, J.A.; Grimes, R.W. Interstitialcy diffusion of oxygen in tetragonal $\text{La}_2\text{CoO}_{4+\delta}$. *Phys. Chem. Chem. Phys.* **2011**, *13*, 2242–2249. [[CrossRef](#)]
93. Seymour, I.D.; Tarancón, A.; Chroneos, A.; Parfitt, D.; Kilner, J.A.; Grimes, R.W. Anisotropic oxygen diffusion in $\text{PrBaCo}_2\text{O}_{5.5}$ double perovskites. *Solid State Ion.* **2012**, *216*, 41–43. [[CrossRef](#)]
94. Anjum, U.; Vashishtha, S.; Agarwal, M.; Tiwari, P.; Sinha, N.; Basu, S.; Haider, M.A. Oxygen anion diffusion in double perovskite $\text{GdBaCo}_2\text{O}_{5+\delta}$ and $\text{LnBa}_{0.5}\text{Sr}_{0.5}\text{Co}_{2-x}\text{Fe}_x\text{O}_{5+\delta}$ ($\text{Ln} = \text{Gd, Pr, Nd}$) electrodes. *Int. J. Hydrogen Energy* **2016**, *41*, 7631–7640. [[CrossRef](#)]
95. Solov'ev, A.L.; Petrenco, E.V.; Omelchenko, L.V.; Vovk, R.V.; Goulati, I.L.; Chroneos, A. Effect of annealing on a pseudogap state in untwinned $\text{YBa}_2\text{Cu}_3\text{O}_{7-\delta}$ single crystals. *Sci. Rep.* **2019**, *9*, 9274. [[CrossRef](#)] [[PubMed](#)]
96. Morales-Zapata, M.A.; Laguna-Bercero, M.A. Lanthanide nickelates for their application on Solid Oxide Cells. *Electrochim. Acta* **2023**, *444*, 141970. [[CrossRef](#)]
97. Kousika, A.; Thomas, T. Defect and migration energies of oxygen vacancies in ABO_2N (A-Ba, Ca, Sr and B-Ta, Nb) perovskite oxynitrides. *Solid State Ion.* **2023**, *399*, 116300. [[CrossRef](#)]
98. Yang, S.G.; Liu, G.C.; Lee, Y.L.; Bassat, J.M.; Gamon, J.; Villegas, A.; Pietras, J.; Zhou, X.D.; Zhong, D. A systematic ab initio study of vacancy formation energy, diffusivity, and ionic conductivity of $\text{Ln}_2\text{NiO}_{4+\delta}$ ($\text{Ln} = \text{La, Nd, Pr}$). *J. Power Sources* **2023**, *576*, 233200. [[CrossRef](#)]
99. Perrichon, A.; Piovano, A.; Boehm, M.; Lemee, M.H.; Ceretti, M.; Paulus, W. Breakdown of the perfect crystal dynamics in dynamically disordered over-stoichiometric $\text{Nd}_2\text{NiO}_{4.25}$. *Phys. Rev. B Cover. Condens. Matter Mater. Phys.* **2023**, *107*, 144303. [[CrossRef](#)]
100. Bamburov, A.; Naumovich, Y.; Khalyavin, D.D.; Yeramchenko, A.A. Intolerance of the Ruddlesden-Popper $\text{La}_2\text{NiO}_{4+\delta}$ Structure to A-Site Cation Deficiency. *Chem. Mater.* **2023**, *35*, 8145–8157. [[CrossRef](#)]
101. Laurencin, J.; Gamon, J.; Flura, A.; Sdanghi, G.; Fourcade, S.; Vibhu, V.; Bassat, J.M. Oxygen diffusion and surface exchange coefficients measurements under high pressure: Comparative behavior of oxygen deficient versus over-stoichiometric air electrode materials. *Fuel Cells* **2023**, *Online*. [[CrossRef](#)]
102. Korte, C.; Schichtel, N.; Hesse, D.; Janek, J. Influence of interface structure on mass transport in phase boundaries between different ionic materials: Experimental studies and formal considerations. *Monatsh. Chem.* **2009**, *140*, 1069–1080. [[CrossRef](#)]
103. Cavallaro, A.; Burriel, M.; Roqueta, J.; Apostolidis, A.; Bernardi, A.; Tarancón, A.; Srinivasan, R.; Cook, S.N.; Fraser, H.L.; Kilner, J.A.; et al. Electronic nature of the enhanced conductivity in YSZ-STO multilayers deposited by PLD. *Solid State Ion.* **2010**, *181*, 592–601. [[CrossRef](#)]
104. Pennycook, T.J.; Beck, M.J.; Varga, K.; Varela, M.; Pennycook, S.J.; Pantelides, S.T. Origin of colossal ionic conductivity in oxide multilayers: Interface induced sublattice disorder. *Phys. Rev. Lett.* **2010**, *104*, 115901. [[CrossRef](#)]

105. Navickas, E.; Huber, T.M.; Chen, Y.; Hetaba, W.; Holzlechner, G.; Rupp, G.; Stöger-Pollach, M.; Friedbacher, G.; Hutter, H.; Yildiz, B.; et al. Fast oxygen exchange and diffusion kinetics of grain boundaries in Sr-doped LaMnO_3 thin films. *Phys. Chem. Chem. Phys.* **2015**, *17*, 7659–7669. [\[CrossRef\]](#) [\[PubMed\]](#)
106. Sun, L.; Marrocchelli, D.; Yildiz, B. Edge dislocation slows down oxide ion diffusion in doped CeO_2 by segregation of charged defects. *Nat. Commun.* **2015**, *6*, 6294. [\[CrossRef\]](#) [\[PubMed\]](#)
107. Saranya, A.M.; Pla, D.; Morata, A.; Cavallaro, A.; Canales-Vazquez, J.; Kilner, J.A.; Burriel, M.; Tarancón, A. Engineering mixed ionic electronic conduction in $\text{La}_{0.8}\text{Sr}_{0.2}\text{MnO}_{3+\delta}$ nanostructures through fast grain boundary oxygen diffusivity. *Adv. Energy Mater.* **2015**, *5*, 1500377. [\[CrossRef\]](#)
108. Saranya, A.M.; Morata, A.; Pla, D.; Burriel, M.; Chiabrera, F.; Garbayo, I.; Hornes, A.; Kilner, J.A.; Tarancón, A. Unveiling the outstanding oxygen mass transport properties of Mn-rich perovskites in grain boundary-dominated $\text{La}_{0.8}\text{Sr}_{0.2}(\text{Mn}_{1-x}\text{Co}_x)_{0.85}\text{O}_{3\pm\delta}$ nanostructures. *Chem. Mater.* **2018**, *30*, 5621–5629. [\[CrossRef\]](#) [\[PubMed\]](#)
109. Kuganathan, N.; Baiutti, F.; Tarancón, A.; Fleig, J.; Chroneos, A. Defects energetics in the SrTiO_3 - LaCrO_3 system. *Solid State Ion.* **2021**, *361*, 115570. [\[CrossRef\]](#)
110. Morgenbesser, M.; Viernstein, A.; Schmid, A.; Herzig, C.; Kubicek, M.; Taibl, S.; Bimashofer, G.; Stahn, J.; Vaz, C.A.F.; Döbeli, M.; et al. Unravelling the Origin of Ultra-Low Conductivity in SrTiO_3 Thin Films: Sr Vacancies and Ti on A-Sites Cause Fermi Level Pinning. *Adv. Funct. Mater.* **2022**, *32*, 2202226. [\[CrossRef\]](#)
111. Maier, J. Nanoionics: Ion transport and electrochemical storage in confined systems. *Nat. Mater.* **2005**, *4*, 805–815. [\[CrossRef\]](#)
112. Gao, Z.; Mogni, L.V.; Miller, E.C.; Railsback, J.G.; Barnett, S.A. A perspective on low-temperature solid oxide fuel cells. *Energy Environ. Sci.* **2016**, *9*, 1602–1644. [\[CrossRef\]](#)
113. Jung, W.C.; Tuller, H.L. A new model describing solid oxide fuel cell cathode kinetics: Model thin film $\text{SrTi}_{1-x}\text{Fe}_x\text{O}_{3-\delta}$ mixed conducting oxides—A case study. *Adv. Energy Mater.* **2011**, *1*, 1184–1191. [\[CrossRef\]](#)
114. Bertei, A.; Yufit, V.; Tariq, F.; Brandon, N.P. A novel approach for the quantification of inhomogeneous 3D current distribution in fuel cell electrodes. *J. Power Sources* **2018**, *396*, 246–256. [\[CrossRef\]](#)
115. Irvine, J.T.S.; Neagu, D.; Verbraeken, M.C.; Chatzichristodoulou, C.; Graves, C.; Mogensen, M.B. Evolution of the electrochemical interface in high-temperature fuel cells and electrolyzers. *Nat. Energy* **2016**, *1*, 15014. [\[CrossRef\]](#)
116. Khan, M.Z.; Song, R.H.; Mehran, M.T.; Lee, S.B.; Lim, T.H. Controlling cation migration and inter-diffusion across cathode/interlayer/electrolyte interfaces of solid oxide fuel cells: A review. *Ceram. Int.* **2021**, *47*, 5839–5869. [\[CrossRef\]](#)
117. Cai, Z.; Kuru, Y.; Han, J.W.; Chen, Y.; Yildiz, B. Surface electronic structure transitions at high temperature on perovskite oxides: The case of strained $\text{La}_{0.8}\text{Sr}_{0.2}\text{CoO}_3$ thin films. *J. Am. Chem. Soc.* **2011**, *133*, 17696–17704. [\[CrossRef\]](#) [\[PubMed\]](#)
118. Kubicek, M.; Cai, Z.H.; Ma, W.; Yildiz, B.; Hutter, H.; Fleig, J. Tensile lattice strain accelerates oxygen surface exchange and diffusion in $\text{La}_{1-x}\text{Sr}_x\text{CoO}_{3-\delta}$ thin films. *ACS Nano* **2013**, *7*, 3276–3286. [\[CrossRef\]](#) [\[PubMed\]](#)
119. Tsvetkov, N.; Lu, Q.; Sun, L.; Crumlin, E.J.; Yildiz, B. Improved chemical and electrochemical stability of perovskite oxides with less reducible cations at the surface. *Nat. Mater.* **2016**, *15*, 1010–1016. [\[CrossRef\]](#) [\[PubMed\]](#)
120. Choi, M.; Ibrahim, I.A.M.; Kim, K.; Koo, J.Y.; Kim, S.J.; Son, J.W.; Han, J.W.; Lee, W. Engineering of Charged Defects at Perovskite Oxide Surfaces for Exceptionally Stable Solid Oxide Fuel Cell Electrodes. *ACS Appl. Mater. Interfaces* **2020**, *12*, 21494–21504. [\[CrossRef\]](#)
121. Zhao, C.; Li, Y.F.; Zhang, W.Q.; Zheng, Y.; Loo, X.M.; Yu, B.; Chen, J.; Chen, Y.; Liu, M.L.; Wang, J.C. Heterointerface engineering for enhancing the electrochemical performance of solid oxide cells. *Energy Environ. Sci.* **2020**, *13*, 53–85. [\[CrossRef\]](#)
122. Riedl, C.; Schmid, A.; Nenning, A.; Summerer, H.; Smeraczek, S.; Schwarz, S.; Bernardi, J.; Optiz, A.; Limbeck, A.; Fleig, J. Outstanding oxygen reduction kinetics of $\text{La}_{0.6}\text{Sr}_{0.4}\text{FeO}_{3-\delta}$ surfaces decorated with platinum nanoparticles. *J. Electrochem. Soc.* **2020**, *167*, 070526. [\[CrossRef\]](#)
123. Perry Murray, E.; Barnett, S.A. ($\text{La},\text{Sr}\text{MnO}_3$)-(Ce,Gd) O_{2-x} composite cathodes for solid oxide fuel cells. *Solid State Ion.* **2001**, *143*, 265–273. [\[CrossRef\]](#)
124. Wang, B.; Yi, J.; Winnubst, L.; Chen, C. Stability and oxygen permeation behavior of $\text{Ce}_{0.8}\text{Sm}_{0.2}\text{O}_{2-\delta}$ - $\text{La}_{0.8}\text{Sr}_{0.2}\text{CrO}_{3-\delta}$ composite membrane under large oxygen partial pressure gradients. *J. Memb. Sci.* **2006**, *286*, 22–25. [\[CrossRef\]](#)
125. Yun, C.; Choi, E.M.; Li, W.; Sun, X.; Maity, T.; Wu, R.; Jian, J.; Xue, S.; Cho, S.; Wang, H.; et al. Achieving ferromagnetic insulating properties in $\text{La}_{0.9}\text{Ba}_{0.1}\text{MnO}_3$ thin films through nanoengineering. *Nanoscale* **2020**, *12*, 9255–9265. [\[CrossRef\]](#) [\[PubMed\]](#)
126. Yang, S.M.; Lee, S.; Jian, J.; Zhang, W.R.; Lu, P.; Jia, Q.X.; Wang, H.Y.; Noh, T.W.; Kalinin, S.V.; MacManus-Driscoll, J.L. Strongly enhanced oxygen ion transport through samarium-doped CeO_2 nanopillars in nanocomposite films. *Nat. Commun.* **2015**, *6*, 8588. [\[CrossRef\]](#) [\[PubMed\]](#)
127. Cho, S.; Yun, C.; Tappertzhofen, S.; Kursumovic, A.; Lee, S.; Lu, P.; Jia, Q.X.; Fan, M.; Jian, J.; Wang, H.Y.; et al. Self-assembled oxide films with tailored nanoscale ionic and electronic channels for controlled resistive switching. *Nat. Commun.* **2016**, *7*, 1. [\[CrossRef\]](#) [\[PubMed\]](#)
128. Huang, J.; MacManus-Driscoll, J.L.; Wang, H. New epitaxy paradigm in epitaxial self-assembled oxide vertically aligned nanocomposite thin films. *J. Mater. Res.* **2017**, *32*, 4054–4066. [\[CrossRef\]](#)
129. Chen, A.; Su, Q.; Han, H.; Enriquez, E.; Jia, Q. Metal Oxide Nanocomposites: A Perspective from Strain, Defect, and Interface. *Adv. Mater.* **2018**, *1803241*, e1803241. [\[CrossRef\]](#) [\[PubMed\]](#)

130. Yoon, J.; Cho, S.; Kim, J.H.; Lee, J.; Bi, Z.X.; Serquis, A.; Zhang, X.H.; Manthiram, A.; Wang, H.Y. Vertically Aligned Nanocomposite Thin Films as a Cathode/Electrolyte Interface Layer for Thin-Film Solid Oxide Fuel Cells. *Adv. Funct. Mater.* **2009**, *19*, 3868–3873. [[CrossRef](#)]
131. Cho, S.; Kim, Y.N.; Lee, J.; Manthiram, A.; Wang, H. Microstructure and electrochemical properties of $\text{PrBaCo}_2\text{O}_{5+\delta}/\text{Ce}_{0.9}\text{Gd}_{0.1}\text{O}_{1.95}$ vertically aligned nanocomposite thin film as interlayer for thin film solid oxide fuel cells. *Electrochim. Acta* **2012**, *62*, 147–152. [[CrossRef](#)]
132. Dubbink, D.; Koster, G.; Rijnders, G. Growth mechanism of epitaxial YSZ on Si by Pulsed Laser Deposition. *Sci. Rep.* **2018**, *8*, 5774. [[CrossRef](#)]
133. Yang, Y.; Bao, H.; Ni, H.; Ou, X.; Wang, S.; Lin, B.; Feng, P.; Ling, Y. A novel facile strategy to suppress Sr segregation for high-entropy stabilized $\text{La}_{0.8}\text{Sr}_{0.2}\text{MnO}_{3-\delta}$ cathode. *J. Power Sources* **2021**, *482*, 228959. [[CrossRef](#)]
134. Ramesh, R.; Schlom, D.G. Creating emergent phenomena in oxide superlattices. *Nat. Rev. Mater.* **2019**, *4*, 257–268. [[CrossRef](#)]
135. Konyshcheva, E.; Francis, S.M.; Irvine, J.T.S. Crystal Structure, Oxygen Nonstoichiometry, and Conductivity of Mixed Ionic-Electronic Conducting Perovskite Composites with CeO_2 . *J. Electrochem. Soc.* **2010**, *157*, B159. [[CrossRef](#)]
136. Lovett, A.J.; Wells, M.P.; He, Z.H.; Lu, J.J.; Wang, H.Y.; MacManus-Driscoll, J.L. High ionic conductivity in fluorite δ -bismuth oxide-based vertically aligned nanocomposite thin films. *J. Mater. Chem. A* **2022**, *10*, 3478–3484. [[CrossRef](#)]
137. Lovett, A.J.; Kursumovic, A.; Dutton, S.; Qi, Z.M.; He, Z.H.; Wang, H.Y.; MacManus-Driscoll, J.L. Lithium-based vertically aligned nanocomposite films incorporating $\text{Li}_x\text{La}_{0.32}(\text{Nb}_{0.7}\text{Ti}_{0.32})\text{O}_3$ electrolyte with high Li^+ ion conductivity. *APL Mater.* **2022**, *10*, 051102. [[CrossRef](#)]
138. Das, D.; Sanchez, F.; Barton, D.J.; Tan, S.S.; Shutthanandan, V.; Devaraj, A.; Ramana, C.V. Rationally engineered vertically aligned $\beta\text{-Ga}_{2-x}\text{W}_x\text{O}_3$ nanocomposites for self-biased solar-blind ultraviolet photodetectors with ultrafast response. *Adv. Mater. Technol.* **2023**, *8*, 2300014. [[CrossRef](#)]
139. Grieshammer, S.; Momenzadeh, L.; Belova, I.V.; Murch, G.E. Ionic and thermal conductivity of pure and doped ceria by molecular dynamics. *Solid State Ion.* **2020**, *355*, 115424. [[CrossRef](#)]
140. Sadykov, V.; Pikalova, E.; Eremeev, N.; Shubin, A.; Zilberberg, I.; Prosvirin, I.; Sadovskaya, E.; Bukhtiyarov, A. Oxygen transport in Pr nickelates: Elucidation of atomic-scale features. *Solid State Ion.* **2020**, *344*, 115155. [[CrossRef](#)]
141. Schutt, J.; Schultze, T.K.; Grieshammer, S. Oxygen ion migration and conductivity in $\text{LaSrGa}_3\text{O}_7$ melillites from first principles. *Chem. Mater.* **2020**, *32*, 4442–4450. [[CrossRef](#)]
142. Namgung, Y.; Hong, J.; Kumar, A.; Lim, D.-K.; Song, S.-J. One step infiltration induced multi-cation oxide nanocatalyst for load proof SOFC application. *Appl. Catal. B* **2020**, *267*, 118374. [[CrossRef](#)]
143. Namgung, Y.; Kumar, A.; Hong, J.; Kim, I.-H.; Song, S.-J. Unraveling the problem associated with multi-cation oxide formation using urea based infiltration techniques for SOFC application. *J. Alloys Compds.* **2021**, *852*, 157037. [[CrossRef](#)]
144. Kildgaard, J.V.; Hansen, H.A.; Vegge, T. DFT plus U study of strain-engineered CO_2 reduction on a CeO_{2-x} (111) facet. *J. Phys. Chem. C* **2021**, *125*, 14221–14227. [[CrossRef](#)]
145. Kim, C.S.; Park, K.W.; Tuller, H.L. Electrochemically controlled defect chemistry: From oxygen excess to deficiency. *Acta Mater.* **2021**, *211*, 116866. [[CrossRef](#)]
146. Leong, Z.Y.; Desai, P.; Morley, N. Can empirical biplots predict high entropy oxide phases? *J. Compos. Sci.* **2021**, *5*, 311. [[CrossRef](#)]
147. Chiabrera, F.; Baiutti, F.; Diercks, D.; Cavallaro, A.; Aguadero, A.; Morata, A.; Taranton, A. Visualizing local fast ionic conduction pathways in nanocrystalline lanthanum manganite by isotope exchange-atom probe tomography. *J. Mater. Chem. A* **2022**, *10*, 2228–2234. [[CrossRef](#)]
148. Zhang, M.; Du, Z.H.; Zhang, Y.; Zhao, H.L. Progress of perovskites as electrodes for symmetrical solid oxide fuel cells. *ACS Appl. Energy Mater.* **2022**, *5*, 13081–13095. [[CrossRef](#)]
149. Pikalova, E.Y.; Kalinina, E.G.; Pikalova, N.S.; Filonova, E.A. High-Entropy Materials in SOFC Technology: Theoretical Foundations for Their Creation, Features of Synthesis, and Recent Achievements. *Materials* **2022**, *15*, 8783. [[CrossRef](#)] [[PubMed](#)]
150. Maity, S.R.; Ceretti, M.; De Barros, R.; Keller, L.; Schefer, J.; Cervellino, A.; Velamazan, J.A.R.; Paulus, W. Large-scale oxygen order phase transitions and fast ordering kinetics at moderate temperatures in $\text{Nd}_2\text{NiO}_{4+\delta}$ electrodes. *Mater. Adv.* **2023**, *4*, 651–661. [[CrossRef](#)]
151. Kala, J.; Anjum, U.; Mani, B.K.; Haider, M.A. Controlling surface cation segregation in a double perovskite for oxygen anion transport in high temperature energy conversion devices. *Phys. Chem. Chem. Phys.* **2023**, *25*, 22022. [[CrossRef](#)]
152. Kabanova, N.A.; Morkhova, Y.A.; Antonyuk, A.V.; Frolov, E.I. Prospective oxygen-ion conductors $\text{Ln}_a\text{X}_b\text{O}_z$: Geometry and energy calculations. *Solid State Ion.* **2023**, *391*, 116142. [[CrossRef](#)]

Disclaimer/Publisher’s Note: The statements, opinions and data contained in all publications are solely those of the individual author(s) and contributor(s) and not of MDPI and/or the editor(s). MDPI and/or the editor(s) disclaim responsibility for any injury to people or property resulting from any ideas, methods, instructions or products referred to in the content.